ANALYSIS OF CHD-7 DEFECTIVE DAUER NEMATODES IMPLICATES COLLAGEN MISREGULATION IN CHARGE SYNDROME FEATURES

Diego Martín Jofré[1*], Dane Kristian Hoffman[2*§], Ailen S. Cervino[3], McKenzie Grundy[2], Sijung Yun[4], Francis Raj Gandhi Amrit[5], Donna Beer Stolz[6], Esteban Salvatore[7], Fabiana Alejandra Rossi[8], Arjumand Ghazi[5,9] , M. Cecilia Cirio[3], Judith L. Yanowitz[2,10#], Daniel Hochbaum[1#]

[*]authors contributed equally

Co-corresponding authors

[1] Departamento de Biodiversidad y Biología Experimental. FCEN. Universidad de Buenos Aires. Buenos Aires, Argentina.
[2] Magee-Womens Research Institute, Pittsburgh, PA, USA
[3] Instituto de Fisiología, Biología Molecular y Neurociencias (IFIBYNE-UBA-CONICET), Facultad de Ciencias Exactas y Naturales, Universidad de Buenos Aires (UBA). Buenos Aires, Argentina.
Institute
[4] Laboratory of Molecular Biology, National Institute of Diabetes and Digestive and Kidney Diseases, National Institutes of Health, Bethesda, Maryland, USA.
[5] Department of Pediatrics, University of Pittsburgh School of Medicine. Pittsburgh, PA, USA.
[6] Center for Biologic Imaging, University of Pittsburgh Medical School. Pittsburgh, PA, USA.
[7] mAbxience S.A.U. Buenos Aires, Argentina.
[8] Instituto de Investigaciones en Medicina Traslacional (IIMT) - CONICET, Universidad Austral. Pilar, Buenos Aires, Argentina.
[9] Departments of Developmental Biology and Cell Biology & Physiology, University of Pittsburgh School of Medicine. Pittsburgh, PA, USA.
[10] Departments of Obstetrics, Gynecology & Reproductive Sciences; Developmental Biology; Microbiology and Molecular Genetics; and the Hillman Cancer Center, University of Pittsburgh, Pittsburgh, PA, USA.

[§]Current Address: Department of Cancer & Cell Biology. Baylor College of Medicine. Houston, Texas, USA.

***Correspondence:** Correspondence should be addressed to

Dr. Daniel Hochbaum
Ciudad Universitaria. Intendente Guiraldes 2160, 4 piso. Laboratorio 79
CABA, Buenos Aires
C1428BGA
Argentina
hochbaumd@bg.fcen.uba.ar
+54 (11) 5285 8658

Dr. Judith Yanowitz
Magee-Womens Research Institute
204 Craft Avenue
Pittsburgh, PA
15213
United States of America

Conflict of Interest

The authors declare no conflicts of interest

ABSTRACT

CHARGE syndrome is a complex developmental disorder caused by mutations in the chromodomain helicase DNA-binding protein7 (CHD7) and characterized by retarded growth and malformations in the heart and nervous system. However, despite the public health relevance of this disorder, relevant targets of CHD7 that relate to disease pathology are still poorly understood. Here we report that *chd-7*, the nematode ortholog of CHD7, is required for dauer morphogenesis, lifespan determination, and stress response. Genetic epistasis placed *chd-7* in the TGF-β pathway. Consistent with our discoveries, we found *chd-7* to be allelic to *scd-3*, a previously identified dauer suppressor from the TGF-β pathway. Interestingly, DAF-12 transcriptionally upregulated *chd-7*, which is necessary to repress *daf-9* for execution of the dauer program. Transcriptomic analysis comparing *chd-7*–defective and normal dauers showed enrichment of collagen genes, consistent with a conserved role for the TGF-β pathway in expression of the extracellular matrix. To validate a conserved function for *chd-7* in vertebrates, we used *Xenopus laevis* embryos, an established model to study craniofacial development. Morpholino mediated knockdown of Chd7 led to embryonic lethality, a reduction in *col2a1* mRNA levels and craniofacial defects in tadpoles. Both lethality and malformations were partially rescued in Chd7-depleted embryos by over-expression of *col2a1*. We suggest that pathogenic features of CHARGE syndrome caused by Chd7 mutations, such as craniofacial malformations, result from the reduction of collagen levels. These studies establish *C. elegans* as an amenable animal model to study the etiology of the developmental defects associated with pathogenic Chd7.

Keywords: CHARGE Syndrome, *C. elegans*, dauer, longevity, TGF-β, Col2a1

INTRODUCTION

CHARGE syndrome is a rare and severe neurodevelopmental disorder that affects the neural tube and neural crest cell derivatives, leading to hypogonadism, heart defects and craniofacial anomalies among other features (1). Inactivating mutations in *CHD7* (chromodomain-helicase-DNA binding 7) are the predominant cause of CHARGE, accounting for greater than 90% of the cases (2). *CHD7* is also mutated in Kallmann syndrome, a milder neurodevelopmental disorder with features overlapping with CHARGE, including impaired olfaction and hypogonadism (3). Exome sequencing studies in patients with autism spectrum disorders (ASDs) identified recurrent disruptive mutations in *CHD8* (4). The CHD proteins comprise a highly conserved family of SNF2-related ATP-dependent chromatin remodelers that are involved in chromatin remodeling and transcriptional regulation (5). Despite the public health relevance of these cognitive disorders, functionally relevant targets of CHD7/8 that relate to disease pathology are still poorly understood. The development of fly, fish and mouse models of CHARGE has abetted in characterization of associated dysfunction, but our understanding of the underlying pathology of CHARGE is still incomplete (6–11). CHD-7 is the ortholog of human CHD7 and CHD8 in *Caenorhabditis elegans*. It contains an ATPase/SNF2 domain and two chromodomains for nucleosome interaction and is the only worm homolog of the Class III CHD proteins, which contain a signature BRK domain (Brahma and Kismet domain) (Figure 1E).

When *C. elegans* encounter crowding, starvation, or high temperature during early development, worms can halt reproductive programs to enter an alternative larval stage known as dauer. Dauers are long-lived, highly stress resistant, and exhibit altered motility and metabolism (12–15). Upon return to normal growth conditions, the larvae exit dauer and develop into fertile adults. Study of dauer formation mutants has provided fundamental insights into pathways affecting longevity, neurodevelopment, metabolism, autophagy and neurodegeneration (12, 15–18).

The DAF-2/insulin/IGF-1 (IIS) signaling pathways controls the dauer entry decision by coupling external cues with neuroendocrine signaling (19). In favorable

126 conditions, DAF-2 activity initiates a conserved kinase cascade, leading to
127 phosphorylation and inhibition of the transcription factor DAF-16/FOXO. In harsh
128 environments, a decrease in the activity of DAF-2 and downstream components of
129 the pathway leads to activation of DAF-16 and causes animals to arrest as dauers
130 (20, 21). In addition to the DAF-2 pathway, DAF-7/ TGFβ also regulates dauer
131 development (22). When worms sense suitable conditions for reproductive
132 development, ASI neurosensory cells secrete DAF-7, which binds to DAF-1/4
133 receptors leading to activation and phosphorylation of the R-SMAD complex DAF-
134 8/14, promoting reproductive programs and inhibiting the pro-dauer complex
135 composed of the SMAD protein DAF-3 and repressor DAF-5. Conversely, absence
136 of DAF-7 leads to activation of the DAF-3/DAF-5 complex to promote dauer entry
137 (23, 24).

138 DAF-7/TGF-β like and DAF-2/IIS pathway were initially described as parallel
139 pathways to regulate dauer entry (25), but recent observations suggest a strong
140 positive feedback between these pathways for dauer entry and longevity (15–20).
141 First, decreased signaling through the TGF-β pathway leads to differential
142 expression of many DAF-16 regulated genes with functions in longevity and dauer
143 entry, such as SOD-3 or insulin peptides. This cross-activation of target genes may
144 be important to amplify weak signals from each sensory pathway to make an all-or-
145 none decision to enter dauer (26–28). Second, the longevity of *daf-2* mutants can be
146 blocked or enhanced by *daf-5* and *daf-3*, respectively, suggesting that transcriptional
147 components of the TGF-β can modulate IIS-dependent longevity genes. Third, for
148 dauer development, *daf-16* is epistatic to *daf-7/8/14 daf-c* mutants (28, 29). Lastly,
149 both signaling pathways converge on *daf-9* and *daf-12* to integrate outputs for
150 diapause entry (30, 31). Central to dauer entry decision is the nuclear receptor DAF-
151 12, which integrates IIS and TGF-β signaling pathways (32). (33) In chromatin
152 immunoprecipitation (ChIP)-chip studies, we identified *chd*-7 as a DAF-12 target
153 gene whose loss caused defective execution of dauer morphogenesis programs.

154

155 We show that while CHD-7 can modulate multiple IIS-associated processes,
156 including *daf-2(e1370)* longevity and immunity. Our epistatic experiments place *chd-*
157 *7* in the TGF-β/DAF-7 pathway. Whole genome mRNA expression profiling of partial
158 dauers show that *chd-7* mutants fail to repress *daf-9* expression during dauer
159 development, preventing developmental arrest of the constitutive dauer mutant *daf-*
160 *7(e1372)*. In addition, we found collagens to be the most differentially regulated
161 genes, consistent with a known role for the TGFβ pathway in regulating components
162 of the extracellular matrix (34).To validate a conserved function for *chd-7* in
163 vertebrates and study the relevance of our results for CHARGE etiology, we used
164 *Xenopus laevis*. Disruption of *Chd7* function in *Xenopus* embryos results in
165 craniofacial defects that mimic CHD-dependent pathological phenotypes (35, 36).
166 We demonstrate that Chd7 regulates expression of the collagen type-II, alpha 1,
167 *col2a1*, the main collagen protein of cartilage (37). Interestingly, craniofacial
168 malformations and embryonic lethality due to *Chd7* knockdown can be rescued by
169 *col2a1* expression. These findings suggest a conserved function of *Chd7*/*chd-7* in
170 regulation of extracellular matrix components and raise the intriguing possibility that
171 defects in collagen expression may contribute to the craniofacial defects seen in
172 CHD7/8-dependent syndromes.
173
174 **RESULTS**
175
176 ***chd-7* functions in development of the dauer larva.**
177 Previously, we identified ~3000 potential DAF-12 target genes by ChIP-chip (32).
178 We reasoned that among these genes would be novel regulators of dauer
179 development. To identify such genes, we took advantage of the temperature-
180 sensitive, constitutive dauer (Daf-c) allele of *daf-2(e1371)*. At the non-permissive
181 temperature of 25°, all the offspring enter the dauer phase and become SDS
182 resistant (20). We reasoned that targets of DAF-12 that function in dauer formation
183 should suppress the Daf-c phenotype of *daf-*2 and produce either defective, SDS-
184 sensitive “partial” dauers or reproductive adults. Screening for RNAi clones that led
185 to development of SDS-sensitive offspring in the more severe *daf-2(e1370)* mutant
186 background, we discovered that *chd-7* RNAi produced arrested, SDS sensitive

187 larvae, indicative of the partial dauer phenotype (38). While typically the dauer larva
188 has an axial ratio (length:width) of nearly 30:1 (20), the partial dauers resulting from
189 *chd-7(RNAi)* exhibited a significant reduction of these proportions and appeared to
190 have defects in radial constriction of the dauer cuticle (Figure 1A and B). By using a
191 transcriptional reporter, we confirmed a strong upregulation of *chd-7* by DAF-12
192 (Figure 1C and D).
193
194 To further validate our screen, we crossed *daf-2(e1370)* worms with three *chd-7*
195 deletion alleles available from the Nematode Knockout Consortia (39). Allele *chd-*
196 *7(tm6139)* contains a 594bp deletion that generates a frame shift and premature
197 stop codon, eliminating all known protein domains (Figure 1E). As shown in Figure
198 1D, SDS-sensitive dauers are obtained when double mutants are grown at 25°C,
199 validating our screen. Comparison of two partial deletion alleles uncovered a critical
200 role for the BRK domain in dauer formation. The *chd-7(gk290)* allele contains an
201 859bp deletion that spans the BRK domain and introduces a frameshift that
202 eliminates the last 356aa. The *chd-7(gk306)* deletion is slightly more C-terminal,
203 truncating the protein immediately after the BRK domain (Figure 1E). When crossed
204 into *daf-2(e1370)* worms, *chd-7(gk306)* develops normal, SDS-resistant dauer
205 larvae, whereas *chd-7(gk290)* formed partial dauers, that are sensitive to detergent
206 (Figure 1F). Importantly, a translational reporter expressing CHD-7::GFP (Figure
207 1F) rescued the "partial dauer" phenotypes observed in *chd-7(gk290);daf-2(e1370)*
208 and *chd-7(tm6139);daf-2(e1370)* mutants.
209
210 The dauer larva is characterized by a slim physique because of a reduction in the
211 volume of epidermal tissues, including the hypodermis, seam cells and XXX cells. In
212 addition, the epidermal tissues produce the dauer cuticle, which confers protection
213 against external damage and dehydration. Because of this cuticle stiffness,
214 hypodermal seam cells fuse to produce the alae, which are bilateral ridges that
215 facilitate body motion. Dauers also switch their metabolism to accumulate lipids to
216 survive for longer periods (40). To further characterize the nature of the defects in
217 the *chd-7*-induced partial dauers, we first studied the cuticle by scanning electro

218 microscopy (SEM) and the adherent junction-associated protein marker AJM-
219 1::GFP. As shown in Figure 1E, partial dauers fail to fuse seam cells, leading to a
220 defective dauer alae. Next we used Oil Red O to examine fat storage and found that
221 unlike other partial dauer mutants (17), the *chd-7;daf-2* abnormal dauers did not
222 exhibit fat-storage deficiencies (Supplementary Figure 1). During the dauer stage,
223 the germ cells remains quiescent to protect their reproductive capacity (41). We
224 observed that germ line in *chd-7* mutant dauers was substantially larger than in
225 dauers and appeared to arrest with an L3-like germ line morphology (Figure 1F).
226 Therefore, we conclude that major morphological changes that occur during dauer
227 larvae formation fail to be executed in *chd-7* mutants including radial constriction of
228 the body, SDS resistance, a developmentally-arrested germ line and presence of
229 dauer alae.
230
231 ***chd-7* is required for *glp-1(e2144)* and *daf-2(e1370)* longevity**
232 In addition to dauer development, the IIS pathway also regulates longevity (12).
233 Thus, we sought to investigate whether *chd-7* also has roles in the determination of
234 lifespan. First, we compared survival of wild-type (N2) worms with two *chd-7* alleles
235 and found that the dauer-suppressor allele *chd-7(gk290)* significantly shortens
236 lifespan, whereas *chd-7(gk306)* had only a marginal effect on longevity (Figure 2A).
237 Surprisingly, a CHD-7::GFP rescue transgene also reduced N2 lifespan (Figure 2B),
238 suggesting that *chd-7* copy number can influence longevity. We then analyzed how
239 *chd-7* affects longevity of IIS mutants. Remarkably, the dauer suppressor allele *chd-*
240 *7(gk290),* but not *chd-7(gk306),* shortened the lifespan extension of daf-2 mutants to
241 an extent comparable with the null allele of *daf-16,* the key IIS downstream target
242 (Figure 2C) (12). Furthermore, *daf-2* longevity is fully restored by CHD-7::GFP
243 (Figure 2D).

244 To determine if the effects on lifespan were specific to the IIS pathway, we also
245 assayed the contribution of *chd-7* to the longevity of germ cell-less animals. *glp-*
246 *1(e2144)* animals are long-lived due to the absence of proliferative germ cells (42).
247 This lifespan extension is dependent on *chd-7* as *chd-7(gk290);glp-1(e2144)* double

248 mutants have a mean lifespan significantly shorter than *glp-1(e2144)* single mutants
249 (Figure 2E).

250 In addition to longevity, IIS reduction also enhances resistance against multiple
251 stressors including pathogen attack and starvation. We asked if chd-7 inactivation
252 also impaired daf-2 mutant's immunoresistance. As shown in Figure 2F, *chd-7*
253 mutants repressed the increased survival of *daf-2* worms upon exposure to the
254 opportunistic pathogen *Pseudomonas aeruginosa* strain PA14 (43). In contrast, *chd-*
255 *7* has a modest effect on survival of wild-type worms' pathogen resistance.
256 Furthermore, the *chd-7(gk290)* allele reduces the survival of starved *daf-2(e1370)* L1
257 larvae (Supplemental Figure 3) (44). Taken together, these results suggest that *chd-*
258 *7* mediates the increased lifespan of at least two longevity paradigms (IIS mutants
259 and germ cell-less animals) as well as the survival response to pathogens and
260 starvation.

261 **CHD-7 belongs to the TGF-β pathway**

262 Genetic analyses implicated *chd-7* as a dauer defective mutant (Daf-d) in the IIS
263 signaling pathway (Figure 1). We sought to understand whether *chd-7* has also roles in
264 the TGF-β dauer pathway (25, 26). While *chd-7(gk290); daf-2(e1370)* and *chd-*
265 *7(tm6139);daf-2(e1370)* arrest as partial dauers at the restrictive temperature of 25°C,
266 double mutants with *daf-7(e1372)* totally bypass the dauer developmental arrest to
267 become fertile adults (Figure 3A). Interestingly, *daf-7*-dependent arrest is recapitulated
268 at higher temperatures (26.5°C), suggesting that *chd-7* has a Hid (high temperature-
269 induced dauer formation) phenotype (45). As expected for a putative transcriptional
270 regulator, epistasis analysis place CHD-7 downstream the receptor DAF-1 and the R-
271 Smad DAF-14 (Figure 3B).
272

273 In addition to dauer formation, the TGF-β signaling pathway also regulates body size
274 and male tale development, mainly through the DBL-1 ligand (46, 47). We compared
275 the length of *chd-7* young adults and found them to be significantly shorter than N2
276 (Figure 3C). We also observed that males carrying the severe loss of function allele
277 *chd-7(tm6139)* fail to mate with *fog-2* mutants (Figure 3D) due to defects in male tail

278 development (not shown). This male infertility is rescued by the CHD-7::GFP transgene.
279
280 More than twenty years ago, in a screen for suppressors of dauer formation within the
281 TGF-β pathway, *Inoue et al* identified three complementation groups (29). We noticed
282 that one of these, *scd-3* (suppressor of constitutive dauer 3), was located between *unc-*
283 *11* and *dpy-5* on chromosome I, in the same genetic region as *chd-7*. *scd-3(sa253)*
284 phenotypes include low brood size, Egl (egg-laying defects), Dpy (weak short body
285 shape) and Mab (Male abnormal), phenotypes shared with *chd-7*. To determine if *chd-7*
286 and *scd-3* are allelic, we sequenced *scd-3(sa253)* and found a single G/A mutation in
287 exon 8 of *chd-7*, that introduces a premature STOP codon at position Q2422,
288 eliminating the BRK domain (Figure 1E).
289
290 **Transcriptomics analysis identifies collagens as targets of CHD-7**
291 To gain further insight into the role of CHD-7 in dauer development, we performed RNA-
292 Seq on *daf-2(e1370)* dauers and *chd-7(gk290);daf-2(e1370)* partial dauers. We
293 analyzed differentially expressed genes (DEGs) and found decreased expression of 28
294 genes and increased expression of 56 genes in double mutants (adjusted p-value by
295 Benjamini Hochberg's False Discovery Rate (FDR)<0.05) (Figure 4A). Among the latter
296 group, we found the *daf-9* cytochrome p450, which integrates inputs from TGF-β and
297 insulin/IGF-I pathways to regulate *daf-12* activity (48). While RNA-seq reads for this
298 gene were marginally detected in *daf-2* dauers, partial dauers exhibited a significantly
299 increased number of reads (Figure 4B). Because *chd-7* loss promotes *daf-9*
300 upregulation in partial dauers (Figure 3A), we hypothesized that expression levels must
301 be critical in the decision to develop as fertile adults or to enter diapause and that the
302 increased expression of *daf-9* in the *chd-7;daf-2* double mutants was preventing full
303 execution of the dauer program. Consistent with this hypothesis, we found that
304 depletion of *daf-9* in *chd7*;*daf-7* animals restored dauer entry at the non-permissive
305 temperature of 25°C (Figure 4C). Thus, the inability of *chd-7* mutants to fully repress
306 *daf-9* is sufficient to inhibit the developmental arrest of TGF-β mutants.
307
308 Transcriptomics analysis showed that 10% of the DEGs are collagens (*col-103*, *col-50*,

309 *dpy-2*, *col-184*, *col-141*, *col-142*, *col-42* and *dpy-9*), which are structural components of
310 the cuticle. This is not surprising due to the conserved role of the TGF-β pathway in
311 regulation of the extracellular matrix (ECM) components, such as fibronectins and
312 collagens (34). Recently, Liu *et al* performed transcriptomic analysis of TGF-β mutants
313 during diapause entry and found both *daf-9* downregulation and misexpression of
314 multiple collagens, supporting our finding that CHD-7 functions within the TGF-β
315 signaling pathway (27).
316
317 **Chd7 regulates *col2a1* during *Xenopus* embryogenesis**
318
319 The partial dauer larvae that arise from knockdown of *chd*-7 are short and thin and lack
320 the dauer alae, indicative of cuticle defects (Figure 1G). Type-II collagen is an ECM
321 protein conserved in all multicellular animals, which forms fibrils (49) and have
322 fundamental roles in development and tissues homeostasis (50). In vertebrates, the
323 fibrillar type-II collagen is the major structural protein of cartilage and plays a prominent
324 role in cranial development in multiple organisms (37, 51). Collagen, type-II, alpha 1
325 (Col2a1) is the major component of the cartilage matrix having a structural function and
326 being an important extracellular signaling molecule for regulation of chondrocyte
327 proliferation, metabolism and differentiation (52–54). The African frog *Xenopus laevis* is
328 a well-established model to study vertebrate facial disorders which often arise from
329 defects in neural crest development and migration (36). In *Xenopus* embryos, prior
330 studies established that Chd7 regulates neural crest specification and migration and its
331 depletion recapitulates the craniofacial defects seen in CHARGE patients (35). To
332 investigate a conserved mechanism of action for Chd7 regulating collagen in
333 vertebrates, we used a previously validated morpholino to induce Chd7 knockdown
334 (*chd7*-MO) (35). In *Xenopus,* Col2a1 is essential for normal development of the skeleton
335 and its expression is restricted to the cartilaginous skeleton of the embryo and adult frog
336 (55). We first analyzed *col2a1* expression by RT-qPCR in *chd7*-MO injected embryos
337 and observed a significant reduction upon morpholino injection (Figure 5A). For targeted
338 disruption of Chd7 function, we injected the dorsal-animal (D1) blastomeres of 8-cell
339 stage embryos fated to contribute to the dorsal anterior structures. *In situ* hybridization
340 of unilaterally injected embryos confirmed a reduction of *col2a1* expression in the

341 branchial arches (55) upon *Chd7* depletion (Figure 5B). The injection of *chd7*-MO into
342 both D1 blastomeres of 8-cell stage embryos with doses between 1.25 ng and 5 ng
343 showed 10-15% embryonic mortality. In contrast, 10 ng led to more than 50% lethality
344 (data not shown and Figure 5C). We sought to investigate if mortality was related to
345 collagen deficits and conducted rescue experiments co-expressing *Xenopus col2a1*
346 mRNA. As shown in Figure 5C, co-injection of *col2a1* mRNA improves embryo survival
347 relative to those injected with *chd7*-MO alone. We then asked if ectopic *col2a1* mRNAs
348 could overcome craniofacial defects associated with *chd7* loss-of-function. We
349 examined the eye size and eye distance as microthalmia and midline defects are often
350 associated with CHARGE syndrome (56) and are recapitulated in *Xenopus* embryos
351 (35). Both eye size and eye distance are reduced in Chd7-depleted embryos and
352 partially rescued by *col2a1* mRNA expression (Figure 5D and 5E). Therefore,
353 expression of *col2a1* ameliorates the phenotypes associated with pathogenic Chd7
354 suggesting that collagen is an important target of this helicase.
355
356 **DISCUSSION**
357 We initially identified *chd*-7 in chromatin immunoprecipitation (ChIP)-chip studies of the
358 nuclear receptor DAF-12 (32), a transcription factor regulating worm aging,
359 development and dauer formation (57), and found it to be critical for *daf-2* mediated
360 dauer development. Comparison of the *chd-7* alleles *gk290* and *gk306* shows a critical
361 role for the BRK domain in dauer development and longevity. In CHARGE patients,
362 deletions or mutations within the BRK domains of Chd7 are sufficient to elicit all the
363 features characteristic of the disease underscoring the importance of this domain (58).
364 The phenotypic differences between the worm alleles highlight the potential of the worm
365 to delimit functional domains of CHD-7 that contribute to disease pathology. In mice,
366 homozygous mutations in *Chd7* lead to embryonic lethality at E10.5, in part because
367 *Chd7* is necessary for early brain development (35). In worms, the presumptive null
368 alleles c*hd-7(tm6139)* and *scd-3(sa253)* were viable but showed reproductive defects,
369 such as improper gonad proliferation and migration, reduced fecundity, male tail defects
370 and hermaphrodite vulval defects (Supplemental Figure 5 and (29)) indicating that *C.*
371 *elegans* are more able to tolerate loss of CHD-7 than mice or humans. Thus, our

372 studies establish *C. elegans* as an amenable animal model to study developmental
373 defects and postnatal features observed in pathogenic Chd7.
374
375 Both a *chd-7* mutation and CHD-7 overexpression shortened the lifespan of otherwise
376 wild-type worms suggesting that the CHD-7 levels must be tightly regulated to ensure
377 proper development. Of note, CHD7 is the most commonly amplified gene in tumors
378 amongst the CHD superfamiliy members, and its overexpression is associated with
379 aggressive subtypes of breast cancer, high tumor grade and poor prognosis (59). Thus,
380 in humans, as well as worms, there are gain-of-function phenotypes associated with
381 Chd7/*chd-7* overexpression. While outside the scope of this work, a CHD-7
382 overexpression strain could be instrumental for modeling CHD7-dependent tumor
383 progression.
384
385 Genetic epistasis analyses place CHD-7 downstream of the TGFβ-like DAF-7, the type I
386 receptor DAF-1, and the R-SMAD DAF-14 placing CHD-7 at the level of the Co-Smad
387 DAF-3 and the Sno/Ski repressor DAF-5 which are also Daf-d. 4. While *daf-3* and *daf-5*
388 completely suppress dauer formation in a *daf-7* background at 25°, both genes fail to
389 suppress dauer formation in TGF-β mutants at 27°C (13, 38) supporting a role for CHD-
390 7 at the DAF-3/DAF-5 step in the pathway. While DAF-3 and DAF-5 work together to
391 control dauer entry, they have opposite effects on *daf-2*-induced longevity: *daf-3*
392 enhances *daf-2(e1370)* longevity while *daf-5* mutations suppresses it (28). We observed
393 that *chd-7* suppresses *daf-2* longevity (Figure 2C), like *daf-5(e1386)*. Together these
394 data suggest that CHD-7 either regulates *daf-5* expression or directly interacts with
395 DAF-5 to regulate downstream target genes or both. In mice, CHD7 was shown to
396 physically interact with SMAD1 and form a transcriptional complex with SMAD4, the
397 mammalian ortholog of DAF-3 (60). We therefore speculate that DAF-3, DAF-5, and
398 CHD-7 may be in ternary complex that regulates *daf-9* expression for dauer entry
399 (Figure 4C). Interactome mapping of the TGF-β pathway also identified SWSN-1, a
400 SWI/SNF subunit component of the BAF complex, as a physical interactor of DAF-3
401 (61). CHD7 interacts with human and Xenopus PBAF (polybromo- and BRG1-
402 associated factor-containing complex) to control neural crest gene expression (35). In

403 worms, both *swsn-1* and *chd-7* fail to develop normal dauers in *daf-2* and *daf-7* mutants
404 (Supplemental Figure 4 and (62)). Thus, we envision that CHD-7 may work together
405 with the BAF complex and DAF-3/DAF-5 to control gene expression of targets genes
406 critical for dauer formation.
407
408 DAF-9 activity is necessary and sufficient for the decision to enter diapause; reduced
409 activity of TGF-β and insulin/IGF-I pathways leads to *daf-9* repression and dauer
410 development. Conversely, *daf-9* expression in the hypodermis is sufficient to inhibit
411 diapause, driving reproductive programs of *daf-7* mutants (27, 30). Ectopic *daf-9*
412 expression drives reproductive programs in the weak *daf-2(e1368)* allele, but only
413 partially suppresses *daf-2(e1370)* diapause animals which arrest at as L3 or early
414 L4, (30). Based on these observations, we speculate that *daf-9* misexpression
415 explains a subset of the *chd-7* phenotypes observed herein, including the partial
416 dauer phenotype, gonad migration defects, and vulval protrusions, all of which
417 overlap with published *daf-9* phenotypes (30, 31, 63). Interestingly, *daf-9* is both
418 upstream and downstream of *daf-12* for dauer formation *(30, 31)*. We show here that
419 DAF-12 regulates *chd-7* expression and that CHD-7 in turn regulates *daf-9*
420 expression. Therefore, we propose that CHD-7 belongs to the transcriptional
421 complex that regulates the feedback loop between *daf-12* and *daf-9*. Moreover, we
422 found increased expression of the *eak-4* paralog F14H8.2 in partial dauers (Figure
423 4A). High activity of this gene may prevent dauer entry by increasing DAF-9 activity
424 (64).
425
426 Among the differentially expressed genes, we note the presence of several G protein
427 coupled receptors (GPCRs), which could be candidate chemoreceptors for dauer
428 pheromone or environmental cues and may be required for either dauer entry or
429 maintenance (42). Consistent with this, we observed that the *chd-7* partial dauers
430 resume reproductive development significantly faster than normal dauers when
431 returned to 16°C. Consistent with our transcriptomic studies, *Liu et al.* analyzed the
432 expression differences between L2/L3 larvae and TGF-β mutants undergoing

433 diapause and found enrichment of collagen genes, GPCRs and *daf-9*, further
434 validating our placement of *CHD-7* in the TGF-β dauer signaling pathway (27).
435
436
437 The expression profiles of adult TGF-β and IIS mutants show a significant
438 overlapping and co-regulation of many DAF-16 target genes. Indeed, the DAF-16-
439 associated element (DAE), is found overrepresented in TGF-β regulated genes (26).
440 We analyzed DAF-16 (L4) and CHD-7 (YA) CHIP-seq data generated by the
441 Modencode project (65) and found both transcriptional regulators to share a
442 significant number of genes (Supplemental Figure 5). This, along with our
443 observation that chd-7 is necessary of lifespan extension of daf-2 mutants, indicates
444 that *chd-7* modulates longevity by regulation of the IIS pathway.
445
446 In *C. elegans*, the TGF-β family pathway has diversified and has unique ligands and
447 effectors for the control of dauer induction and aspects of somatic development.
448 Mutations in the TGF-β ligand *dbl-1* and its downstream components cause a small
449 body size (Sma phenotype) (47, 66). Consistent with *chd-7* being a component of the
450 TGF-β signaling pathway, *chd-7(gk290)* and *chd-7(tm6139)* are significantly shorter
451 than wild-type worms. This phenotype is also observed in *scd-3* mutants (29). The *dbl-1*
452 pathway mutants have defects in male tale development (47), a phenotype shared in
453 *scd-3* (29) and *chd-7* mutant animals (data not shown and (29)). Therefore, our results
454 suggest that CHD-7 acts as a regulator of both the *daf-7* and *dbl-1* branches of the
455 TGF-β pathway. The short body length of *dbl-1(ev580)* animals is partially rescued by
456 mutations in the collagen gene *lon-3*, a component of the *C. elegans* cuticle.
457 Interestingly, *lon-3* expression depends on the *dbl-1* pathway, suggesting that in worms
458 and in vertebrates, the TGF-β pathway regulates extracellular matrix components, such
459 as collagens (34, 67).
460
461 Craniofacial anomalies seen in CHARGE patients involve tissues deriving from cells of
462 the neural crest, including craniofacial cartilage and bone, heart, ears and eyes (56, 68).
463 *Xenopus laevis* is an established model to understand fundamental questions of

464 craniofacial biology (36). *chd7* knockdown in frogs and more recently demonstrated in
465 zebrafish (11, 35), leads to defects in neural crest specification and migration, which
466 was recently recapitulated in human embryonic stem cells (hESCs) (69). Our RNA-seq
467 analysis revealed that CHD-7 regulates expression of genes from the cuticle, a modified
468 extracellular matrix (70). Here, we show a conserved role for Chd7 in regulating *col2a1*
469 expression, a type II collagen and the major component of cartilage (51). While
470 additional studies are required, we speculate that Chd7 could regulate *col2a1* in a
471 complex with the transcription factor Sox10 (71, 72) or through the TGF-β signaling
472 pathway (34, 73). Supporting the latter mechanism, it was demonstrated recently that
473 TGF-β regulates *col2a1* expression in chondrocytes (74). Taken together, our data
474 supports a model in which collagen misexpression by pathogenic Chd7 leads to
475 craniofacial defects and embryonic lethality.
476
477 **METHODS**
478
479 ***C. elegans* strains**
480 All strains were grown and maintained on standard nematode growth medium (NGM). In
481 Argentina (Hochbaum lab), plates were supplemented with 0.1mg/ml streptomycin and
482 100U/ml Nystatin using either *E. coli* OP50 or OP50-1 strains as the food source. In
483 Pittsburgh (Yanowitz lab), strains were grown on standard NGM seeded with OP50.
484 Temperature-sensitive strains were maintained at 16°C and shifted to the non-
485 permissive temperature of 25°C to induce dauer formation, unless otherwise indicated.
486 All other strains were maintained at 20°C. All *daf-7* strains were maintained at low
487 density to prevent dauer induction at 16°C. Dauer studies were performed in both the
488 Yanowitz and Hochbaum laboratories to validate results. All *chd-7* alleles were
489 outcrossed at least 5 times prior to use.
490
491 Strains utilized in this study are listed in Supplementary Table 1. Standard genetic
492 crosses were used to make double or triple mutants. The presence of mutant alleles
493 was confirmed a) by the *daf-c* phenotypes in animals heterozygous for additional

494 mutations and b) by PCR and/or sequencing for all additional mutations. Primers and
495 PCR conditions used in this study are shown in Supplemental Table 2.
496
497 **RNAi screen for dauer suppressors**
498 All RNAi clones were picked from the Ahringer bacterial feeding library (75). These *E.*
499 *coli* clones were seeded on NGM plates supplemented with 1mM of IPTG (Isopropyl β-
500 D-1-thiogalactopyranoside) and 0.1µg/ml ampicillin, and used for inducing RNAi by the
501 feeding method (76).
502
503 GL228 [*rrf-3(pk1426)*] II;*daf-2(e1371)* III] eggs were placed in 24-well RNAi plates
504 seeded with bacteria expressing the dsRNA of interest. Worms were maintained for 5
505 days at 15ºC until adulthood, then were transferred to an identical 24-well plate to lay
506 eggs for 5 hours. Adults were removed and the eggs were incubated at 25°C for 4 days
507 to allow formation of dauers. *daf-16(RNAi)* and the empty vector were used as controls.
508 Proper dauer formation was assessed by observation in a dissecting microscope and by
509 1% SDS resistance. RNAi clones that caused abnormal dauer phenotypes were
510 validated in *daf-2(e1370)* worms. Identity of the dsRNA was confirmed by sequencing
511 (Macrogen, Korea).
512
513 ***daf-9* suppression assays**
514 For preparation of *daf-9*(RNAi) plates, bacterial cultures were grown overnight in LB
515 with 10 µg/ml tetracycline and 50 µg/ml carbenicillin and induced with 4 mM IPTG
516 (Isopropyl *β*-d-1-thiogalactopyranoside) for four hours. Cultures were spun down,
517 suspended in 1/10 volume and 30 µl of bacteria were seeded on 3 cm NGM plates
518 made with 1 mM IPTG and 50 µg/ml carbenicillin. Plates were grown overnight at 25°C
519 and stored at 4°C for no more than 2 weeks prior to use.
520
521 L4 stage animals were placed on 3 cm RNAi plates. Two worms per plate were used for
522 *daf-7(e1372)*, while three worms were used for *daf-7; chd-7(gk290)* and *daf-7; chd-*
523 *7(tm6139)*. After 72 hours, the adults were removed and plates were replaced at 25° for
524 2-3 days. The total number of dauers, L4s, and adults were then assessed.

525

526 **SDS survival assay**

527 Young adults were transferred to seeded plates and permitted to lay for 5 days at 25°C.
528 The arrested progeny were then washed off plates with M9 (22 mM KH_2PO_4, 42mM
529 Na_2HPO_4, 85.5 mM NaCl, 1mM $MgSO_4$) into 15 ml glass conical tubes. Collected
530 animals were washed 2-3 times with M9 and the excess liquid was aspirated off.
531 Animals were then treated with 2 ml of 1% SDS for 30 minutes on a nutator at 25 ºC.
532 Following incubation, the samples were washed 3 times with M9 and any excess liquid
533 was aspirated off. Animals were aliquoted to 5 seeded plates with 50-70 worms per
534 plate and allowed to recover at 16°C. The recovered animals were then quantified, and
535 the percentage recovered was calculated. This was repeated 3 times for each strain
536 tested. Comparisons were performed using the χ-squared Test in R; P values were
537 corrected using the Bonferroni method for multiple comparisons.

538

539 ***fog-2* mating assay**

540 To determine if males were capable of siring offspring, 8 males from each strain tested
541 were plated with 4 *fog-2(q71)* adult females on seeded 10 cm plates**.** After 24h, *fog-2*
542 females were transferred to new plates and within 48h the proportion of fertile females
543 were scored. Assay was repeated two times.

544

545 **Lifespan assays**

546 All lifespan experiments were conducted by transferring 1 day-old adults from 15°C to
547 20°C for the remainder of the lifespan assay. NGM plates were seeded with *E. coli*
548 OP50-1 or, for experiments involving gene silencing, with HT115::DE3. ~150 L4
549 hermaphrodites were transferred to 5 plates per experiment. Every 48h, animals were
550 scored as alive, dead or censored (animals that exploded, died from bagging or dried
551 out at the edges of the plates). Animals were considered dead when they did not
552 respond to a soft touch to the head with a pick. To prevent the progeny from interfering
553 with the assay, adults were transferred to fresh plates every 48h until egg production
554 ceased. For *glp-1(e2144)* assays, eggs were kept at 20°C for 4h and then transferred at
555 25.5°C for 72h to induce sterility and switched to 20°C for the remainder of the

556 experiment. Lifespan data were analyzed using the Kaplan-Meier method. Statistics
557 were calculated using the Mantel-Cox nonparametric log-rank method using OASIS2
558 (77).
559
560 **L1 survival**
561 Eggs were obtained by of gravid adults (Worms are mixed by inversion in 5 ml bleach
562 solution, 3.5 ml ddH20, 1.0 ml 5% NaOCl, 0.5 ml 5 N KOH. After the worms have lysed
563 and eggs are released, the eggs were centrifuged, the bleach solution aspirated, and
564 eggs were washed withM9 buffer). After extensive washing, eggs were suspending in
565 Eggs were suspended in 5ml of sterile M9 with 0.1µg/ml of streptomycin and left to
566 hatch at 20°C under gentle shaking for 16h. To normalize population density, resulting
567 L1 larvae were diluted to obtain 1 larva/µl in 5ml of M9 and kept at 20°C under constant
568 agitation for the remainder of the experiment. Every 48h, a 100µl aliquot of L1 larvae
569 were spotted onto a seeded NGM plate and then incubated at 20°C for 72h. Animals
570 were scored as alive that developed beyond the L2 stage. Percentage of the population
571 alive was normalized to day 1 L1 larvae.
572
573 **Pathogen resistance assay**
574 The pathogenic bacterial strain used in this study was *Pseudomonas aeruginosa* (strain
575 PA14). This strain was streaked from a frozen stock onto a LB agar plate, incubated at
576 37°C overnight and then kept at 4°C (shelf-life of one week). For survival assay, a single
577 PA14 colony was inoculated in King's broth and incubated at 37°C overnight with
578 shaking. 20µl of this culture was seeded onto slow killing NGM plates (containing 0.35%
579 peptone instead of 0.25%) and incubated for 24h at 37°C. The plates were then left to
580 sit at room temperature for 24hrs. The following day, 150 L4 hermaphrodites grown at
581 15°C were distributed onto 5 PA14 plates and incubated at 25°C. Survival was
582 monitored at intervals of 6h to 12h and live, dead and censored animals were recorded.
583 Data and statistics were analyzed using the Kaplan-Meier method as described in the
584 section "Lifespan assays".
585
586 **Oil-Red-O (ORO) staining**

587 Dauers grown at 25°C for 5 days were stained for lipids using ORO, as previously
588 described (78). Animals were mounted on a 4% agarose pad and observed in a Zeiss
589 Axioplan brightfield microscope equipped with a Micropublisher 3.3 camera (Q
590 Imaging). Image J (NIH) was used to quantify the amount of lipids in each animal. At
591 least 20 animals of each strain were quantified. Statistical differences were determined
592 by Student's t test.
593
594 **Microscopy and fluorescence imaging**
595 For imaging dauers and adults, worms were immobilized in a 25mM sodium azide
596 solution and imaged at 10x and 20x magnification. Images were collected using a Zeiss
597 Axioplan Imaging Microscope with a DIC system and Zeiss Plan-Neofluar 10x and 20x
598 objectives lens. Images were acquired with a Micropublisher 3.3 camera (Q Imaging).
599 ImageJ (NIH) software was used to quantify worm size.
600
601 For imaging *pCHD-7::mCherry* fluorescence, worms were immobilized with 1mM
602 levamisole on fresh 2% agarose pads and imaged immediately using a Nikon A1r
603 confocal microscope equipped with a 40x PLAN APO oil objective. ImageJ (NIH)
604 software was used to quantify fluorescence intensity.
605
606 For imaging gonads in *daf-2(e1370)* and mutants, young adults were transferred to
607 seeded plates and permitted to lay eggs for 5 days at 25°C to form dauers, then
608 collected and fixed with Carnoy's solution (75µl EtOH, 37.5µl Acetate, 12.5µl
609 Chloroform) and stained with 5mg/ml DAPI (4′,6-diamidino-2-phenylindole) in PBS.
610 Animals were imaged as 0.5µm Z-stacks with the Nikon A1r Confocal Microscope with
611 40x and 60x plan APO oil objectives.
612
613 For imaging *ajm-1::GFP*, young adults were transferred to seeded plates and permitted
614 to lay eggs for 5 days at 25°C to form dauers. The arrested progeny was then washed
615 off plates with M9 into 15 ml glass conical tubes. Collected animals were washed 2-3
616 times with M9 and the excess liquid was aspirated off. Animals were then immobilized

617 with levamisole and the seam cells were imaged as Z-stacks by confocal microscopy as
618 described immediately above.
619
620 For scanning electron microscopy, worms were fixed by immersing in 2.5%
621 glutaraldehyde in PBS for several hours. Worms were washed 3X in PBS then post
622 fixed in aqueous OsO 4 for 1h, then washed 3x in PBS, dehydrated through a graded
623 series of ethanols (30-100%) then chemically dried with 2 x 10 min incubations in
624 hexamethyldisilazane. Dried worms were sprinkled onto copper double stick tape on
625 aluminum stubs, sputter coated with 3.5 nm gold-palladium alloy then evaluated on a
626 JEOL JEM 6335F microscope at 5 kV.
627
628 **Library preparation and RNA-seq**
629 *daf-2(e1370)* and *chd-7(gk290);daf-2(e1370)*, synchronized eggs were kept at 25°C for
630 10 days and resulting dauers were collected and frozen. Total RNA was extracted with
631 TRIzol (Invitrogen) following the kit´s protocol. cDNA library was prepared with NEBNext
632 Ultra II RNA library prep kit for Illumina (New England Biolabs), and the sequencing
633 carried out using Illumina's HiSeq-2500 sequencer with single-end mode and read
634 length of 50 bp. Five replicates for *daf-2(e1370)* vs. *chd-7(gk290);daf-2(e1370)* were
635 sequenced. For data assessment, a quality control with FastQC software (version
636 0.11.5) was used. First the raw reads that aligned against the *E. coli* genome (K12
637 genome) were removed. The remaining sequences were aligned against the reference
638 genome of *C. elegans* WS260 using STAR (version 2.5.4a). The number of mapped
639 reads to genes was counted using Htseq (version 0.9.1). Finally, the DEGs were
640 determined using DESeq2 (version 1.20.0) with a cutoff of 0.05 on False Discovery
641 Rate (FDR). R version 3.5.0 (2018-04-23) and Bioconductor version 3.7 with
642 BiocInstaller version 1.30.0 were used. Heatmaps were generated using pheatmap
643 package (version 1.0.12) with hierarchical clustering on the rows with the default
644 options.
645
646 **Genomic Sequencing of *scd-3***

647 A 6cm plate replete with *scd-3* gravid animals was washed with 1ml M9 and collected in
648 a glass conical. Worms were washed extensively, then placed on the nutator for 1 hour
649 to allow remaining gut bacteria to be passed into the medium. Worms were again
650 washed 3-4 times and settled by gravity. The worm pellet was transferred to 1.5ml
651 Eppendorf and genomic DNA was prepared according to the manufacturer's protocol
652 with the Purelink Genomic DNA Kit (Invitrogen) except that after addition of digestion
653 buffer, worms were pulverized with a microfuge hand dounce prior to incubation at
654 55°C. Sequencing was performed by Psomagen, Qiagen CLC Genomics Workbench
655 was used to align the DNA against WBcel235 and view the variant.
656
657 ***Xenopus laevis* embryo manipulation and microinjections**
658 *Xenopus* embryos were obtained by natural mating. Adult frogs' reproductive behavior
659 was induced by injection of human chorionic gonadotropin hormone. Eggs were
660 collected, de-jellied in 3% cysteine (pH 8.0), maintained in 0.1 X Marc's Modified
661 Ringer's (MMR) solution and staged according to Nieuwkoop and Faber (79). The
662 embryos were placed in 3% ficoll prepared in 1 X MMR for microinjection. Chd7
663 morpholino (*chd7*-MO: 5′-AACTCATCATGCCAGGGTCTGCCAT-3′) (Gene Tools, LLC)
664 specificity has been previously characterized (Bajpai 2010). The cDNA of *Xenopus*
665 *laevis* Col2a1 was amplified by PCR from pCMV-Sport 6-*col2a1* (Dharmacon) with
666 primers M13F and M13R (see Supplemental Table 2). The PCR fragment was digested
667 with *EcoR*V and *Not*I and cloned into pCS2+ previously digested with *Stu*I and *Not*I.
668 Capped mRNAs for *col2a1* were transcribed *in vitro* with SP6 using the mMessage
669 mMachine kit (Ambion) following linearization with *Not*I. *Chd7*-MO and *col2a1* mRNA
670 were injected into both D1 blastomeres of 8-cell staged embryos (80) for lethality and
671 morphometrics analysis. *Chd7*-MO was injected into one D1 blastomeres of 8-cell
672 staged embryos for analysis of *col2a1* expression.
673
674 Whole-mount *in situ* hybridization was carried out as previously described (81). pCMV-
675 Sport 6-*col2a1* (Dharmacon) construct was linearized with *Sal*I and transcribed with T7
676 for antisense probe synthesis. Images of whole embryos were collected with a Leica

677 DFC420 camera attached to a Leica L2 stereoscope. Morphometics analysis were done
678 on fixed embryos using ImageJ software (https://fiji.sc/).
679
680 **RNA preparation and RT-qPCR**
681 For RNA extraction, 2-cell stage embryos were injected into both blastomeres with 5 ng
682 of *chd7*-MO, collected at stage 23 and snap-frozen for later processing. Six embryos
683 were combined for each treatment and RNA was isolated using RNAzol (Sigma-
684 Aldrich). RNA concentration of each sample was measured using a Nanodrop
685 spectrophotometer, and 250 ng of RNA were reverse transcribed using qScript cDNA
686 SuperMix (QuantaBio). Quantitative PCR (qPCR) was preformed using the Forget-Me-
687 Not qPCR Master Mix (Biotium) with a Biorad iCycler thermocycler. Amplification was
688 performed using oligonucleotides designed with PerlPrimer software for *col2a1*
689 (Forward 5´TCCCTGTTGATGTTGAAGCC3´; Reverse 5´-
690 CAATAGTCACCGCTCTTCCA-3´ and ODC primers have been previously described
691 (82) (Forward 5´CAAAGCTTGTTCTACGCATAGCA3´; Reverse
692 5´GGTGGCACCAAATTTCACACT 3´). The relative expression of *col2a1* was
693 normalized to *ODC* expression and determined via the method previously described
694 (83).
695
696 **Ethics Statement**
697 *Xenopus laevis* experiments were carried out in strict accordance with the
698 recommendations in the Guide for the Care and Use of Laboratory Animals of the NIH
699 and also the ARRIVE guidelines. The animal care protocol was approved by the
700 Comisión Institucional para el Cuidado y Uso de Animales de Laboratorio (CICUAL) of
701 the School of Applied and Natural Sciences, University of Buenos Aires, Argentina
702 (Protocol #64).
703
704
705
706
707

Acknowledgments

The authors would like to thank Bruno Moretti, Hernan Grecco and Mario Rossi for experimental support. We also thank the Consejo Nacional de Investigaciones Científicas y Técnicas (CONICET). Diego Martín Jofré is a CONCIET fellow and Daniel Hochbaum is a career investigator from CONICET. DH laboratory was supported by the Agencia Nacional de Promoción Científica y Tecnológica of Argentina (PICT-2016-0269) and Conicet (PIP 1122015 0100731 CO). Funding for this work was also provided by grants from the CHARGE Syndrome Foundation (JLY and DH), The Company of Biologists (MF), NIGMS (R01GM104007 JLY), and NIA (R01AG051659 AG). This work was also supported, in part, by the Intramural Research Program of the NIH and the National Institute of Diabetes and Digestive and Kidney Diseases (SY).

Author roles and contributions

Conceived and designed the experiments: DMJ, DKH, ASC, FAG, ES, MCC, JLY, DH. Performed the experiments: DMJ, DKH, ASC, MG, FRGA, DBS, ES, FAR, DH. Analyzed the data: DMJ, DKH, ASC, SY, FRGA, AG, MCC, JLY, DH. Drafted the manuscript: JLY,DH. Reviewed and edited the manuscript: DMJ, DKH, AG, MCC, JLY, DH.

729 **REFERENCES**

730

731 1. L. E. L. M. Vissers, *et al.*, Mutations in a new member of the chromodomain gene
732 family cause CHARGE syndrome. *Nature genetics* **36**, 955–7 (2004).
733 2. R. Balasubramanian, *et al.*, Functionally compromised CHD7 alleles in patients
734 with isolated GnRH deficiency. *Proc Natl Acad Sci U S A* **111**, 17953–17958 (2014).
735 3. H.-G. Kim, *et al.*, Mutations in CHD7, encoding a chromatin-remodeling protein,
736 cause idiopathic hypogonadotropic hypogonadism and Kallmann syndrome. *Am. J.*
737 *Hum. Genet.* **83**, 511–519 (2008).
738 4. R. Bernier, *et al.*, Disruptive CHD8 Mutations Define a Subtype of Autism Early in
739 Development. *Cell* **158**, 263–276 (2014).
740 5. C. G. A. Marfella, A. N. Imbalzano, The Chd family of chromatin remodelers.
741 *Mutation research* **618**, 30–40 (2007).
742 6. S. A. Patten, *et al.*, Role of Chd7 in Zebrafish: A Model for CHARGE Syndrome.
743 *PLoS One* **7** (2012).
744 7. E. A. Bosman, *et al.*, Multiple mutations in mouse Chd7 provide models for
745 CHARGE syndrome. *Hum Mol Genet* **14**, 3463–3476 (2005).
746 8. C. Tian, *et al.*, Otitis media in a new mouse model for CHARGE syndrome with a
747 deletion in the Chd7 gene. *PloS one* **7**, e34944 (2012).
748 9. G. Daubresse, *et al.*, The Drosophila kismet gene is related to chromatin-
749 remodeling factors and is required for both segmentation and segment identity.
750 *Development* **126**, 1175–1187 (1999).
751 10. D. J. Melicharek, L. C. Ramirez, S. Singh, R. Thompson, D. R. Marenda,
752 Kismet/CHD7 regulates axon morphology, memory and locomotion in a Drosophila
753 model of CHARGE syndrome. *Hum Mol Genet* **19**, 4253–4264 (2010).
754 11. Z. Asad, *et al.*, Rescue of neural crest-derived phenotypes in a zebrafish
755 CHARGE model by Sox10 downregulation. *Hum Mol Genet* **25**, 3539–3554 (2016).
756 12. C. Kenyon, J. Chang, E. Gensch, A. Rudner, R. Tabtiang, A C. elegans mutant
757 that lives twice as long as wild type. *Nature* **366**, 461–464 (1993).
758 13. P. L. Larsen, Aging and resistance to oxidative damage in Caenorhabditis
759 elegans. *Proc Natl Acad Sci U S A* **90**, 8905–8909 (1993).

760 14. M. M. Gaglia, C. Kenyon, Stimulation of Movement in a Quiescent, Hibernation-
761 Like Form of Caenorhabditis elegans by Dopamine Signaling. *J Neurosci* **29**, 7302–
762 7314 (2009).
763 15. J. Wang, S. K. Kim, Global analysis of dauer gene expression in Caenorhabditis
764 elegans. *Development* **130**, 1621–1634 (2003).
765 16. E. Cohen, J. Bieschke, R. M. Perciavalle, J. W. Kelly, A. Dillin, Opposing
766 activities protect against age-onset proteotoxicity. *Science* **313**, 1604–1610 (2006).
767 17. A. Meléndez, *et al.*, Autophagy genes are essential for dauer development and
768 life-span extension in C. elegans. *Science* **301**, 1387–1391 (2003).
769 18. R. Christensen, L. de la Torre-Ubieta, A. Bonni, D. A. Colón-Ramos, A conserved
770 PTEN/FOXO pathway regulates neuronal morphology during C. elegans development.
771 *Development* **138**, 5257–5267 (2011).
772 19. C. A. Wolkow, K. D. Kimura, M.-S. Lee, G. Ruvkun, Regulation of C. elegans
773 Life-Span by Insulinlike Signaling in the Nervous System. *Science* **290**, 147–150 (2000).
774 20. R. C. Cassada, R. L. Russell, The dauerlarva, a post-embryonic developmental
775 variant of the nematode Caenorhabditis elegans. *Dev Biol* **46**, 326–342 (1975).
776 21. D. L. Riddle, P. S. Albert, "Genetic and Environmental Regulation of Dauer Larva
777 Development" in *C. Elegans II*, 2nd Ed., D. L. Riddle, T. Blumenthal, B. J. Meyer, J. R.
778 Priess, Eds. (Cold Spring Harbor Laboratory Press, 1997) (September 25, 2017).
779 22. P. Ren, *et al.*, Control of C. elegans larval development by neuronal expression
780 of a TGF-beta homolog. *Science* **274**, 1389–1391 (1996).
781 23. D. Park, A. Estevez, D. L. Riddle, Antagonistic Smad transcription factors control
782 the dauer/non-dauer switch in C. elegans. *Development* **137**, 477–485 (2010).
783 24. L. S. da Graca, DAF-5 is a Ski oncoprotein homolog that functions in a neuronal
784 TGF pathway to regulate C. elegans dauer development. *Development* **131**, 435–446
785 (2003).
786 25. J. H. Thomas, D. A. Birnby, J. J. Vowels, Evidence for parallel processing of
787 sensory information controlling dauer formation in Caenorhabditis elegans. *Genetics*
788 **134**, 1105–1117 (1993).
789 26. W. M. Shaw, S. Luo, J. Landis, J. Ashraf, C. T. Murphy, The C. elegans TGF-β
790 Dauer Pathway Regulates Longevity via Insulin Signaling. *Current Biology* **17**, 1635–

791 1645 (2007).
792 27. T. Liu, K. K. Zimmerman, G. I. Patterson, Regulation of signaling genes by
793 TGFbeta during entry into dauer diapause in C. elegans. *BMC Dev Biol* **4**, 11 (2004).
794 28. S. D. Narasimhan, *et al.*, PDP-1 Links the TGF-β and IIS Pathways to Regulate
795 Longevity, Development, and Metabolism. *PLoS Genet* **7** (2011).
796 29. T. Inoue, J. H. Thomas, Suppressors of transforming growth factor-beta pathway
797 mutants in the Caenorhabditis elegans dauer formation pathway. *Genetics* **156**, 1035–
798 1046 (2000).
799 30. B. Gerisch, A. Antebi, Hormonal signals produced by DAF-9/cytochrome P450
800 regulate C. elegans dauer diapause in response to environmental cues. *Development*
801 **131**, 1765–1776 (2004).
802 31. H. Y. Mak, G. Ruvkun, Intercellular signaling of reproductive development by the
803 C. elegans DAF-9 cytochrome P450. *Development* **131**, 1777–1786 (2004).
804 32. D. Hochbaum, *et al.*, DAF-12 regulates a connected network of genes to ensure
805 robust developmental decisions. *PLoS Genet* **7**, e1002179 (2011).
806 33. N. Fielenbach, A. Antebi, C. elegans dauer formation and the molecular basis of
807 plasticity. *Genes Dev* **22**, 2149–2165 (2008).
808 34. R. A. Ignotz, J. Massagué, Transforming growth factor-beta stimulates the
809 expression of fibronectin and collagen and their incorporation into the extracellular
810 matrix. *J. Biol. Chem.* **261**, 4337–4345 (1986).
811 35. R. Bajpai, *et al.*, CHD7 cooperates with PBAF to control multipotent neural crest
812 formation. *Nature* **463**, 958–962 (2010).
813 36. A. Dubey, J.-P. Saint-Jeannet, Modeling Human Craniofacial Disorders in
814 Xenopus. *Curr Pathobiol Rep* **5**, 79–92 (2017).
815 37. D. W. Seufert, J. Hanken, M. W. Klymkowsky, Type II collagen distribution during
816 cranial development in Xenopus laevis. *Anat. Embryol.* **189**, 81–89 (1994).
817 38. P. S. Albert, D. L. Riddle, Mutants of Caenorhabditis elegans that form dauer-like
818 larvae. *Dev Biol* **126**, 270–293 (1988).
819 39. E. S. Haag, Dial-a-mutant: web-based knockout collections for model organisms.
820 *Biol. Cell* **99**, 343–347 (2007).
821 40. , Dauer Epithelium (March 24, 2021).

822 41. P. Kadekar, R. Roy, AMPK regulates germline stem cell quiescence and integrity
823 through an endogenous small RNA pathway. *PLoS Biol* **17** (2019).
824 42. H. Hsin, C. Kenyon, Signals from the reproductive system regulate the lifespan of
825 C. elegans. *Nature* **399**, 362–366 (1999).
826 43. D. A. Garsin, *et al.*, Long-lived C. elegans daf-2 mutants are resistant to bacterial
827 pathogens. *Science* **300**, 1921 (2003).
828 44. I. Lee, A. Hendrix, J. Kim, J. Yoshimoto, Y.-J. You, Metabolic rate regulates L1
829 longevity in C. elegans. *PLoS One* **7**, e44720 (2012).
830 45. M. Ailion, J. H. Thomas, Dauer Formation Induced by High Temperatures in
831 Caenorhabditis elegans. *Genetics* **156**, 1047–1067 (2000).
832 46. C. Savage, *et al.*, Caenorhabditis elegans genes sma-2, sma-3, and sma-4
833 define a conserved family of transforming growth factor beta pathway components. *Proc*
834 *Natl Acad Sci U S A* **93**, 790–794 (1996).
835 47. Y. Suzuki, *et al.*, A BMP homolog acts as a dose-dependent regulator of body
836 size and male tail patterning in Caenorhabditis elegans. *Development* **126**, 241–250
837 (1999).
838 48. B. Gerisch, C. Weitzel, C. Kober-Eisermann, V. Rottiers, A. Antebi, A hormonal
839 signaling pathway influencing C. elegans metabolism, reproductive development, and
840 life span. *Dev Cell* **1**, 841–851 (2001).
841 49. R. P. Boot-Handford, D. S. Tuckwell, Fibrillar collagen: the key to vertebrate
842 evolution? A tale of molecular incest. *Bioessays* **25**, 142–151 (2003).
843 50. W. R. Wilcox, Connective Tissue and Its Heritable Disorders: Molecular, Genetic,
844 and Medical Aspects,. *Am J Hum Genet* **72**, 503–504 (2003).
845 51. A. Wood, D. E. Ashhurst, A. Corbett, P. Thorogood, The transient expression of
846 type II collagen at tissue interfaces during mammalian craniofacial development.
847 *Development* **111**, 955–968 (1991).
848 52. N. Garamszegi, *et al.*, Extracellular matrix-induced transforming growth factor-
849 beta receptor signaling dynamics. *Oncogene* **29**, 2368–2380 (2010).
850 53. W. Xin, J. Heilig, M. Paulsson, F. Zaucke, Collagen II regulates chondroycte
851 integrin expression profile and differentiation. *Connect Tissue Res* **56**, 307–314 (2015).
852 54. , Differential effect of ECM molecules on re-expression of cartilaginous markers in

853 near quiescent human chondrocytes - Chiu - 2011 - Journal of Cellular Physiology -
854 Wiley Online Library (March 24, 2021).
855 55. R. Kerney, B. K. Hall, J. Hanken, Regulatory elements of Xenopus col2a1 drive
856 cartilaginous gene expression in transgenic frogs. *Int J Dev Biol* **54**, 141–150 (2010).
857 56. J. R. Siebert, J. M. Graham, C. MacDonald, Pathologic features of the CHARGE
858 association: Support for involvement of the neural crest. *Teratology* **31**, 331–336 (1985).
859 57. A. Antebi, W. H. Yeh, D. Tait, E. M. Hedgecock, D. L. Riddle, daf-12 encodes a
860 nuclear receptor that regulates the dauer diapause and developmental age in C.
861 elegans. *Genes Dev* **14**, 1512–1527 (2000).
862 58. C. L. Hale, A. N. Niederriter, G. E. Green, D. M. Martin, Atypical phenotypes
863 associated with pathogenic CHD7 variants and a proposal for broadening CHARGE
864 syndrome clinical diagnostic criteria. *Am. J. Med. Genet. A* **170**, 344–354 (2016).
865 59. X. Chu, *et al.*, Genotranscriptomic meta-analysis of the CHD family chromatin
866 remodelers in human cancers – initial evidence of an oncogenic role for CHD7. *Mol*
867 *Oncol* **11**, 1348–1360 (2017).
868 60. Y. Liu, *et al.*, CHD7 interacts with BMP R-SMADs to epigenetically regulate
869 cardiogenesis in mice. *Human Molecular Genetics* **23**, 2145–2156 (2014).
870 61. M. Tewari, *et al.*, Systematic Interactome Mapping and Genetic Perturbation
871 Analysis of a C. elegans TGF-ᴺL Signaling Network. *Molecular Cell*, 14.
872 62. C. G. Riedel, *et al.*, DAF-16 employs the chromatin remodeller SWI/SNF to
873 promote stress resistance and longevity. *Nat. Cell Biol.* **15**, 491–501 (2013).
874 63. K. Jia, P. S. Albert, D. L. Riddle, DAF-9, a cytochrome P450 regulating C.
875 elegans larval development and adult longevity. *Development* **129**, 221–231 (2002).
876 64. P. J. Hu, J. Xu, G. Ruvkun, Two membrane-associated tyrosine phosphatase
877 homologs potentiate C. elegans AKT-1/PKB signaling. *PLoS Genet.* **2**, e99 (2006).
878 65. S. E. Celniker, *et al.*, Unlocking the secrets of the genome. *Nature* **459**, 927–930
879 (2009).
880 66. C. Savage, *et al.*, Caenorhabditis elegans genes sma-2, sma-3, and sma-4
881 define a conserved family of transforming growth factor 3 pathway components.
882 *Developmental Biology*, 5 (1996).
883 67. Y. Suzuki, G. A. Morris, M. Han, W. B. Wood, A Cuticle Collagen Encoded by the

884 lon-3 Gene May Be a Target of TGF-β Signaling in Determining Caenorhabditis elegans
885 Body Shape. *Genetics* **162**, 1631–1639 (2002).
886 68. X. Huang, J.-P. Saint-Jeannet, Induction of the neural crest and the opportunities
887 of life on the edge. *Developmental Biology* **275**, 1–11 (2004).
888 69. H. Okuno, *et al.*, CHARGE syndrome modeling using patient-iPSCs reveals
889 defective migration of neural crest cells harboring CHD7 mutations. *Elife* **6** (2017).
890 70. J. M. Kramer, "Extracellular Matrix" in *C. Elegans II*, 2nd Ed., D. L. Riddle, T.
891 Blumenthal, B. J. Meyer, J. R. Priess, Eds. (Cold Spring Harbor Laboratory Press,
892 1997) (March 22, 2021).
893 71. T. Suzuki, D. Sakai, N. Osumi, H. Wada, Y. Wakamatsu, Sox genes regulate
894 type 2 collagen expression in avian neural crest cells. *Dev Growth Differ* **48**, 477–486
895 (2006).
896 72. D. He, *et al.*, Chd7 cooperates with Sox10 and regulates the onset of CNS
897 myelination and remyelination. *Nature Neuroscience* **19**, 678–689 (2016).
898 73. A. B. Roberts, B. K. McCune, M. B. Sporn, TGF-β: Regulation of extracellular
899 matrix. *Kidney International* **41**, 557–559 (1992).
900 74. A. Tekari, R. Luginbuehl, W. Hofstetter, R. J. Egli, Transforming Growth Factor
901 Beta Signaling Is Essential for the Autonomous Formation of Cartilage-Like Tissue by
902 Expanded Chondrocytes. *PLOS ONE* **10**, e0120857 (2015).
903 75. R. S. Kamath, J. Ahringer, Genome-wide RNAi screening in Caenorhabditis
904 elegans. *Methods* **30**, 313–321 (2003).
905 76. L. Timmons, D. L. Court, A. Fire, Ingestion of bacterially expressed dsRNAs can
906 produce specific and potent genetic interference in Caenorhabditis elegans. *Gene* **263**,
907 103–112 (2001).
908 77. S. K. Han, *et al.*, OASIS 2: Online application for survival analysis 2 with features
909 for the analysis of maximal lifespan and healthspan in aging research. *Oncotarget* **7**,
910 56147–56152 (2016).
911 78. R. Ratnappan, *et al.*, Germline Signals Deploy NHR-49 to Modulate Fatty-Acid β-
912 Oxidation and Desaturation in Somatic Tissues of C. elegans. *PLoS Genetics* **10**
913 (2014).
914 79. , Normal Table of Xenopus Laevis (Daudin) | Taylor & Francis Group (March 23,

915 2021).
916 80. , Blastomeres show differential fate changes in 8-cell Xenopus laevis embryos
917 that are rotated 90° before first cleavage - Huang - 1998 - Development, Growth &
918 Differentiation - Wiley Online Library (March 23, 2021).
919 81. V. Gawantka, *et al.*, Gene expression screening in Xenopus identifies molecular
920 pathways, predicts gene function and provides a global view of embryonic patterning.
921 *Mechanisms of Development* **77**, 95–141 (1998).
922 82. Q. Cao, Y. Shen, W. Zheng, H. Liu, C. Liu, Tcf7l1 promotes transcription of
923 Kruppel-like factor 4 during Xenopus embryogenesis. *J Biomed Res* **32**, 215–221
924 (2018).
925 83. M. W. Pfaffl, A new mathematical model for relative quantification in real-time
926 RT-PCR. *Nucleic Acids Res* **29**, e45 (2001).
927

928

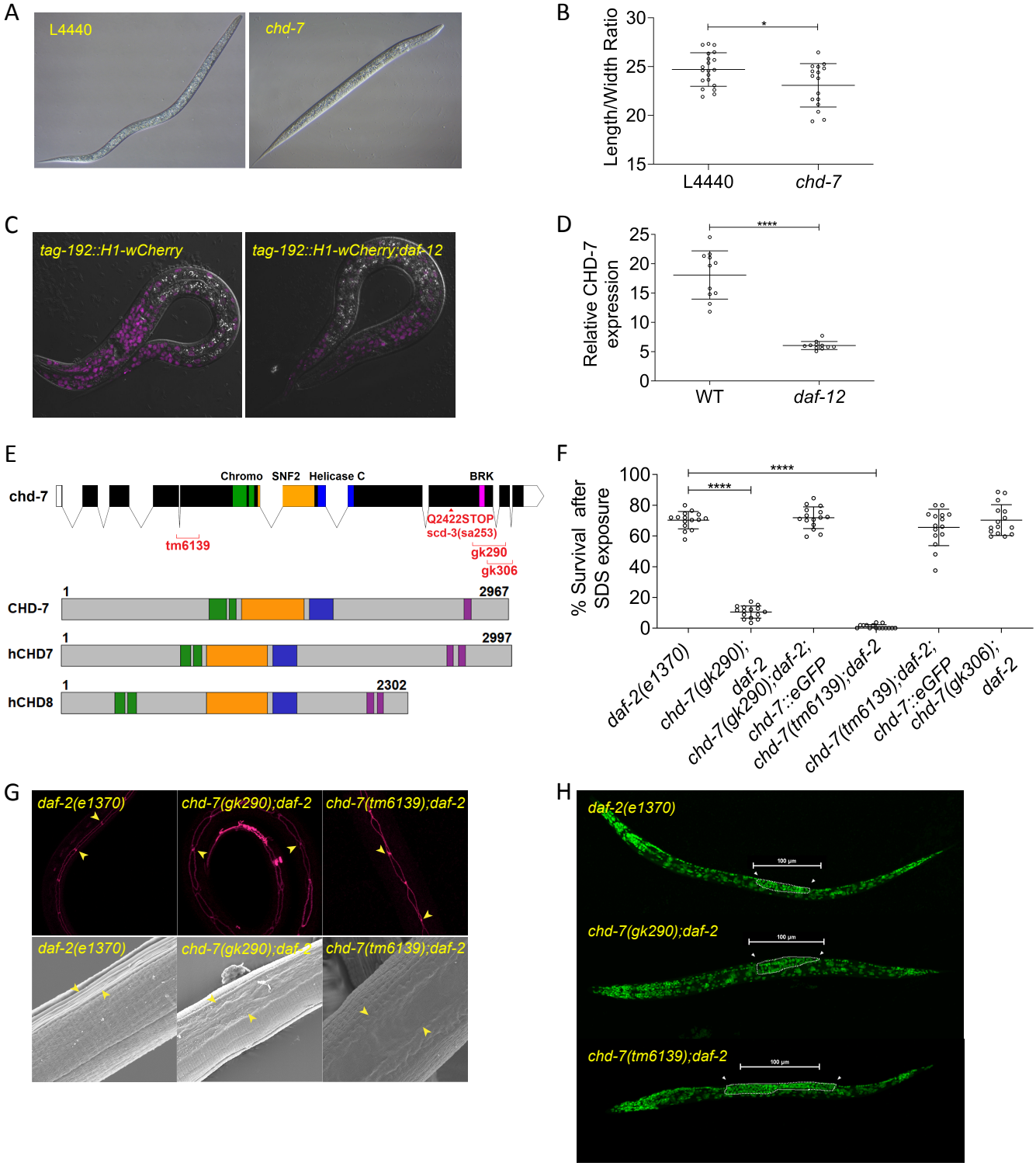

Figure 1: *chd-7*, a CHD superfamily member and a *daf-12* controlled gene, regulates *daf-2* dauer formation. A) *chd-7(RNAi)* causes a partial dauer phenotype in *daf-2(e1370).* Representative DIC photomicrographs of *daf-2(e1370)* normal dauers fed on vector control RNAi at 25°C or the partial dauer phenotype when worms are fed on *chd-7(RNAi)*. **B)** Quantification of the axial ratio. Three biological replicates were scored with 16-21 individual dauers per replicate. Horizontal black lines represent mean with SD. *p<0.05. **C)** *daf-12* regulates *chd-7* expression. Representative images of *tag-192::H1-wCherry* or *tag-192::H1-wCherry; daf-12(rh61rh411)* worms in L2/L3 stage**. D)** Relative expression of the

translational reporter (n>10/strain). Unpaired t test, ****p<0.0001. **E)** *C.elegans chd*-7 gene and proteins. Top: *chd-7* genomic region. UTR and exons shown as bars; introns by lines. In red, available *chd-7* deletional alleles (data obtained from CGC and NBRP). Signature domains in CHD proteins**:** two N-terminal chromodomains for interaction with a variety of chromatin components (green), a SNF-2 like domain with ATPase activity (yellow) and a Helicase domain (blue). The Class III subfamily is defined by a BRK domain (purple). Bottom images depict the predicted protein isoforms of *C. elegans* CHD-7, human CHD7 and human CHD8. **F)** *chd-7*(*gk290*);*daf-2* and *chd-7*(*tm6139*);*daf-2* develop as SDS sensitive dauer larvae. Each dot represents one plate with at least 40 arrested animals per plate and a minimum of 725 total animals per strain tested. Horizontal black lines represent mean percentage with SD. Statistical significance was calculated using Chi-squared test with Bonferroni correction for multiple comparisons. ****p<0.0001. **G)** *chd-7* partial dauers fail to develop the dauer alae. Top row, representative photomicrographs of *daf-2(e1370)* dauers or partial dauers expressing the *ajm-1*::GFP reporter. Arrowheads indicate seam cell junctions. Bottom row, SEM images showing alae details. **H)** Dauer germ cells in *chd-7* mutants keep proliferating. (Top to Bottom) *daf-2(e1370), chd-7(gk290);daf-2, chd-7(tm6139);daf-2.* Representative z-projections for dauer animals stained with DAPI (green). Arrowheads denote the left and right most distal end of the gonad.

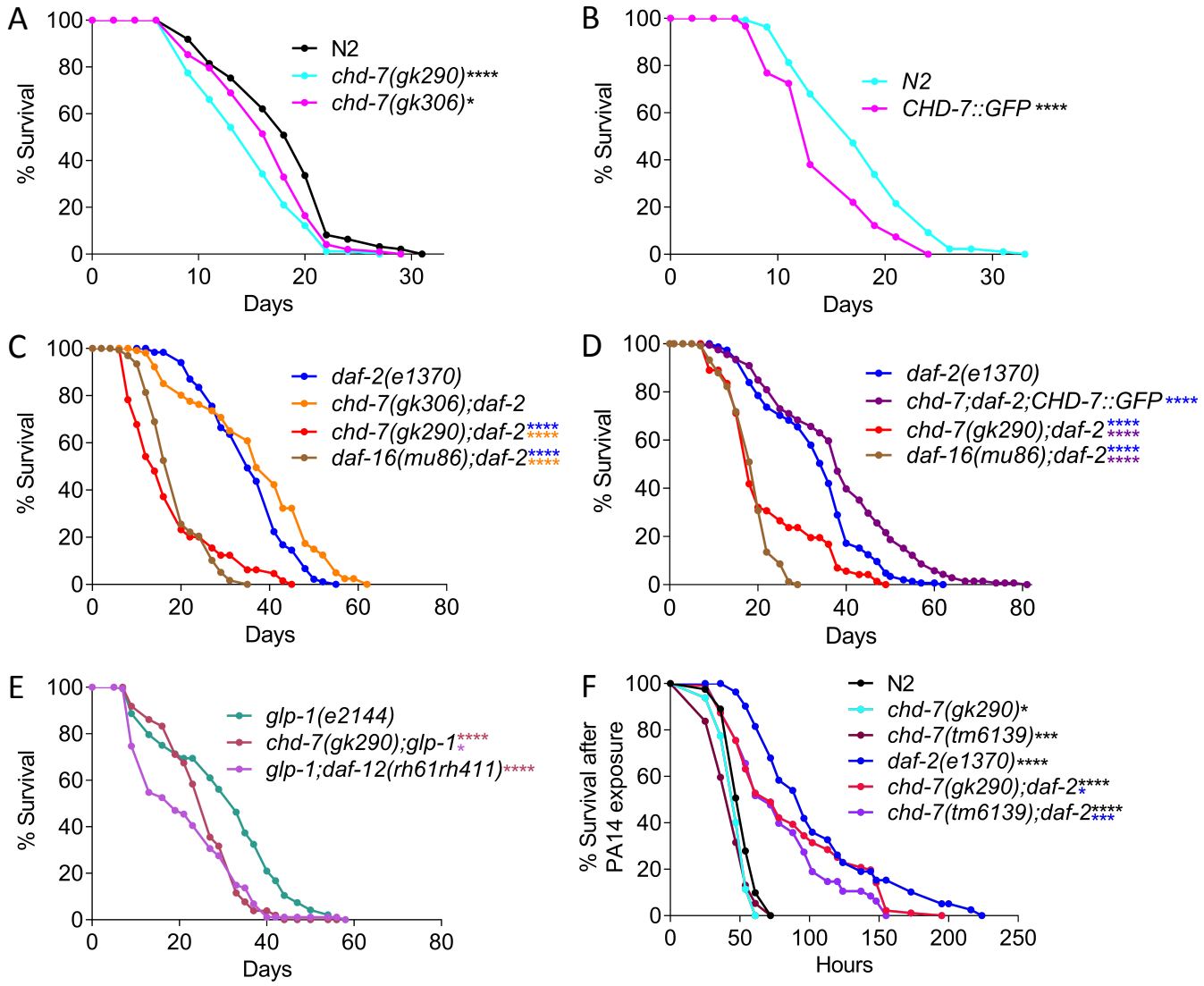

Figure 2: *chd-7* affects longevity and immune response. A-E) *chd-7* promotes longevity in *wild-type*, *daf-2(e1370)* and *glp-1(e2144)* mutants. Mean survival days on OP50-1 **A)** WT (18.12), *chd-7(gk290)* (14.91), *chd-7(gk306)* (16.53) **B)** WT (17.85), CHD-7::GFP (14.35) **C)** *daf-2(e1370)* (35.58), *chd-7(gk306);daf-2* (37.18), *chd-7(gk290);daf-2* (17.47), *daf-16(mu86);daf-2(e1370)* (18.85). **D)** *daf-2(e1370)* (27.9), *chd-7(gk290);daf-2;CHD-7::GFP* (30.84), *chd-7(gk290);daf-2* (19.13), *daf-16(mu86);daf-2* (14.48). **E)** *glp-1(e2144)* (30.4), *chd-7(gk290);glp-1* (28.37), *glp-1;daf-12(rh61rh411)* (25.99). Number of animals and other data from replicate found in Supplementary Table 2. **F)** *chd-7* mediates the immune response against the opportunistic bacteria *P. aeruginosa*. Mean lifespan in hours (m) ± standard error of the mean (SEM). 'n' is the number of animals analyzed/total number in experiment. N2 (m = 52.11 ± 0.96, n = 94/162), *chd-7(gk290)* (m = 47.45 ± 1.05, n = 54.130/), *chd-7(tm6139)* (m = 44.47 ± 1.57, n = 56/80), *daf-2(e1370)* (m = 105.46 ± 5.61, n = 65/115), *chd-7(gk290);daf-2* (m = 86.74 ± 4.21, n = 103/120) and *chd-7(tm6139);daf-2* (m = 79.13 ± 4.9, n = 50/60). In A-F) survival data analyzed using Kaplan−Meier test. *p<0.05 (*), ***p <0.001 and ****p <0.0001. Asterisk´s color represents the strain of reference.

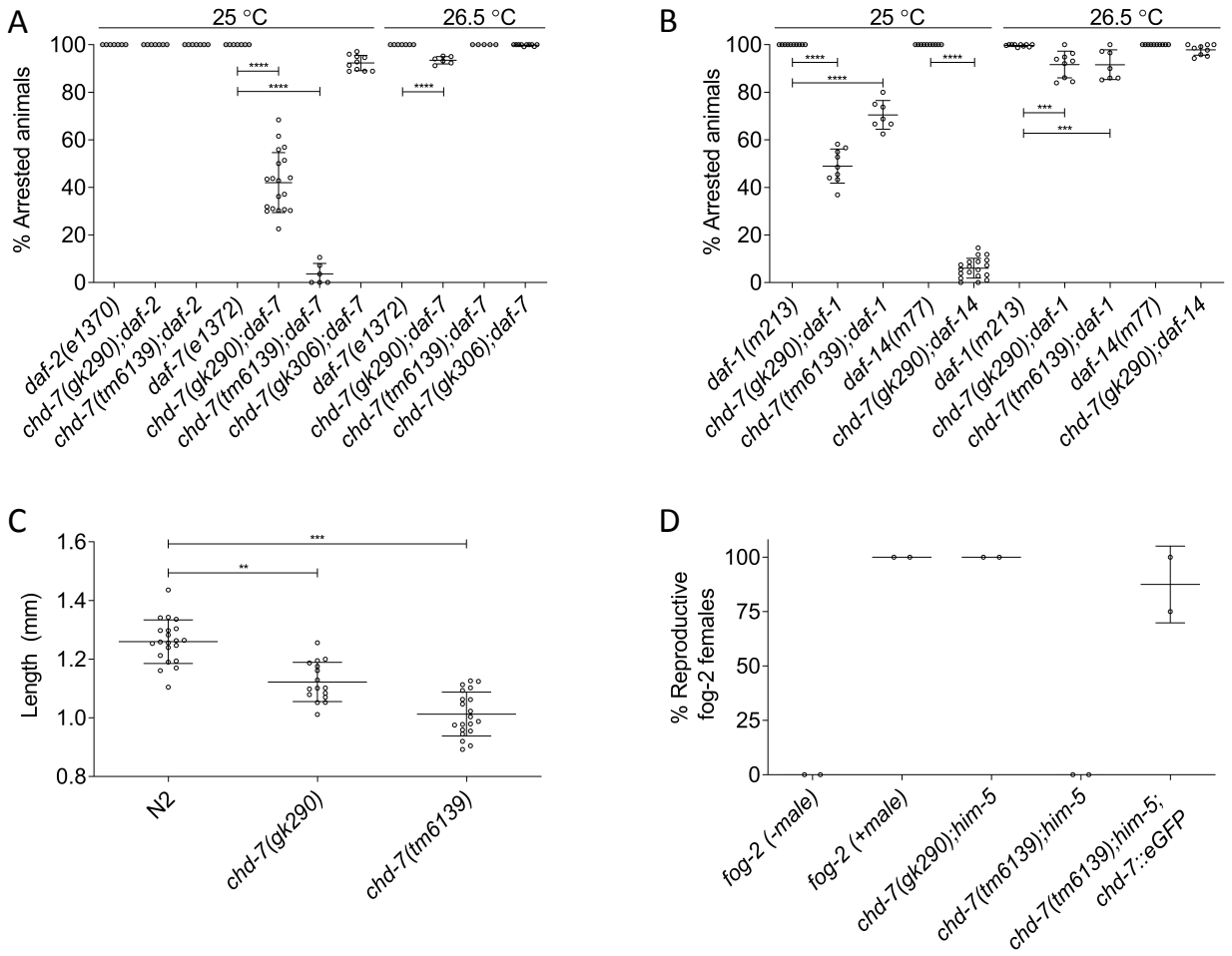

Figure 3: CHD-7 belongs to the TGF-β signaling pathway. A-B) Dauer larva formation of *daf-c;chd-7* mutants. 7 individual L4's were grown on 7 plates at the specified temperature for 1 week and the number of arrested and non-arrested progeny was scored. Each dot represents a plate with at least one progeny and minimum 44 totals animals quantified for each strain. Horizontal black lines represent mean percentage with SD. Statistical significance was calculated using Chi-squared test with Bonferroni correction for multiple comparisons. ****p<0.0001**. C)** CHD-7 regulates body size. Synchronized worms were grown at 20°C until adulthood and length of at least 16 individuals was scored. Statistical significance was calculated using one-way Anova. **p<0.01, ***p<0.001. **D)** *chd-7(tm6139)* males do not mate. 8 male animals from each strain tested were plated with 4 *fog-2* females on 10 cm plates**.** After 24 hrs *fog-2* females were transferred to new plates and within 48h the proportion of fertile females were scored. Assay was repeated two times.

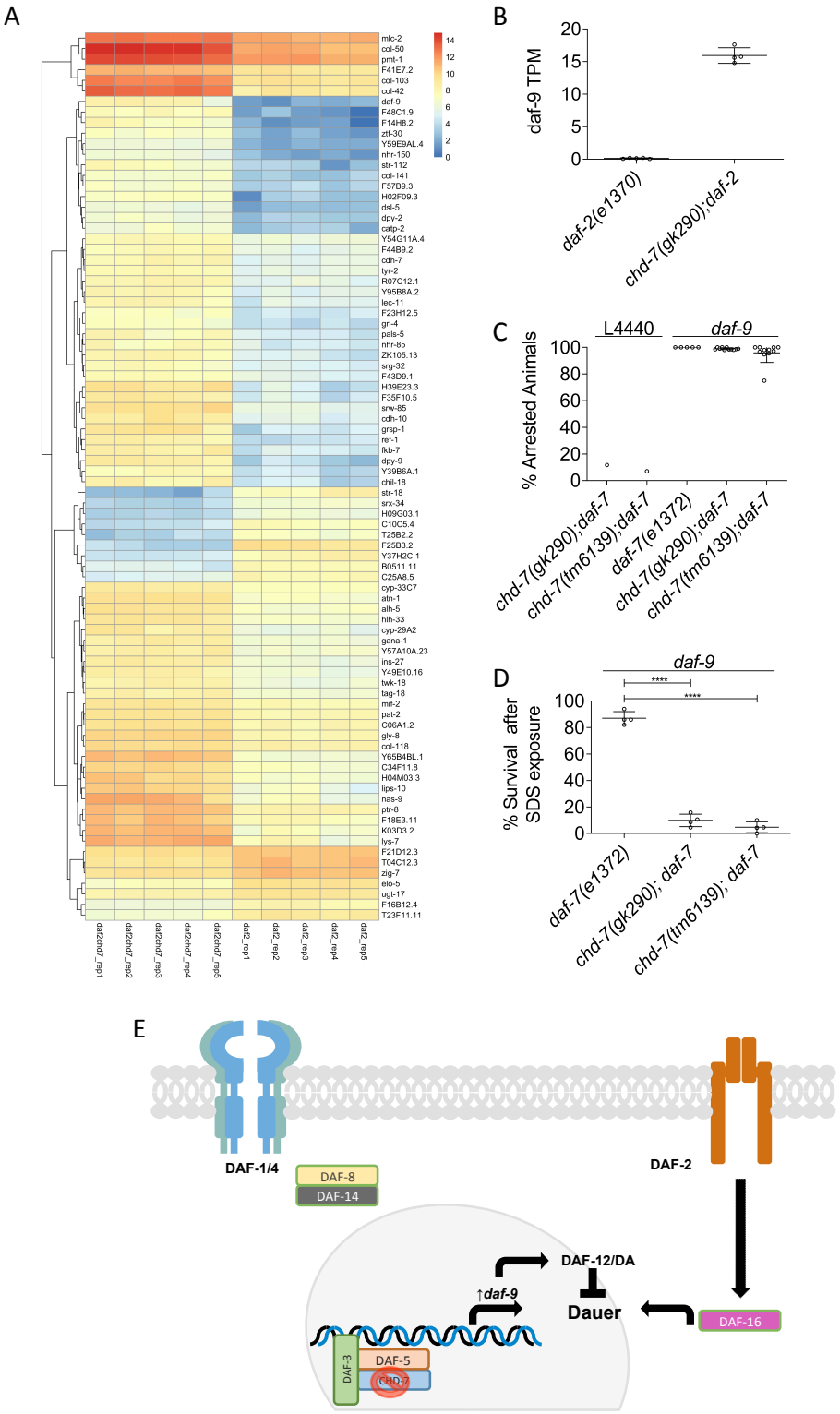

Figure 4: RNA-Seq analysis of transcriptome changes in dauers induced by *chd-7(gk290)* mutant. A) Heat map of individual expression values of all 84 differentially expressed genes (DEGs, cutoff of 0.05 on FDR). Prior to heat map calculation, DEGs were determined using DESeq2 (version 1.20.0). The color scale represents row z-score. Hierarchical clustering of the DEGs is represented by dendrograms at the left. **B)** Partial dauers exhibit an increased number of reads of *daf-9. daf-9* transcripts per million (TPM) were generated and summarized to gene level using Qiagen's CLC Genomics

Workbench Software. Bars represent the SD and Mean. **C)** *daf-9* knockdown in *chd-7*;*daf-7(e1372)* animals rescues dauer arrest at 25°C. 2-3 young L4's were plated on to freshly seeded plates with either *daf-9* or L4440 empty vector RNAi and allowed to lay eggs. After 72h, the adults were removed and the proportion of progeny that arrested as dauers was calculated. Each dot represents a plate of at least 34 animals and a minimum of 598 total animals per strain tested. Horizontal black lines represent mean with SD. Statistical significant differences were determined by one-way ANOVA. **D)** *daf-9* RNAi rescues arrest in *chd-7*;*daf-7(e1372)* animals but leads to incomplete dauers. Arrested animals grown at 25°C on *daf-9* RNAi plates were treated with 1% SDS for 30 min and survival was scored. Each dot represents a plate of at least 30 animals and a minimum of 159 total animals per strain tested. Horizontal black lines represent mean with SD. Statistical significant differences were determined by one-way ANOVA. **E)** Mechanism of action for *chd-7* in dauer development. In dauering conditions, CHD-7 forms a transcriptional complex with DAF-3/DAF-5 to repress *daf-9* expression. In *chd-7* mutants, *daf-9* expression prevents dauer formation driven by reduced activity of both DAF-7/TGF-β and DAF-2/IIS signaling pathways, presumably by binding dafachronic acids (DA) and subsequent activation of DAF-12.

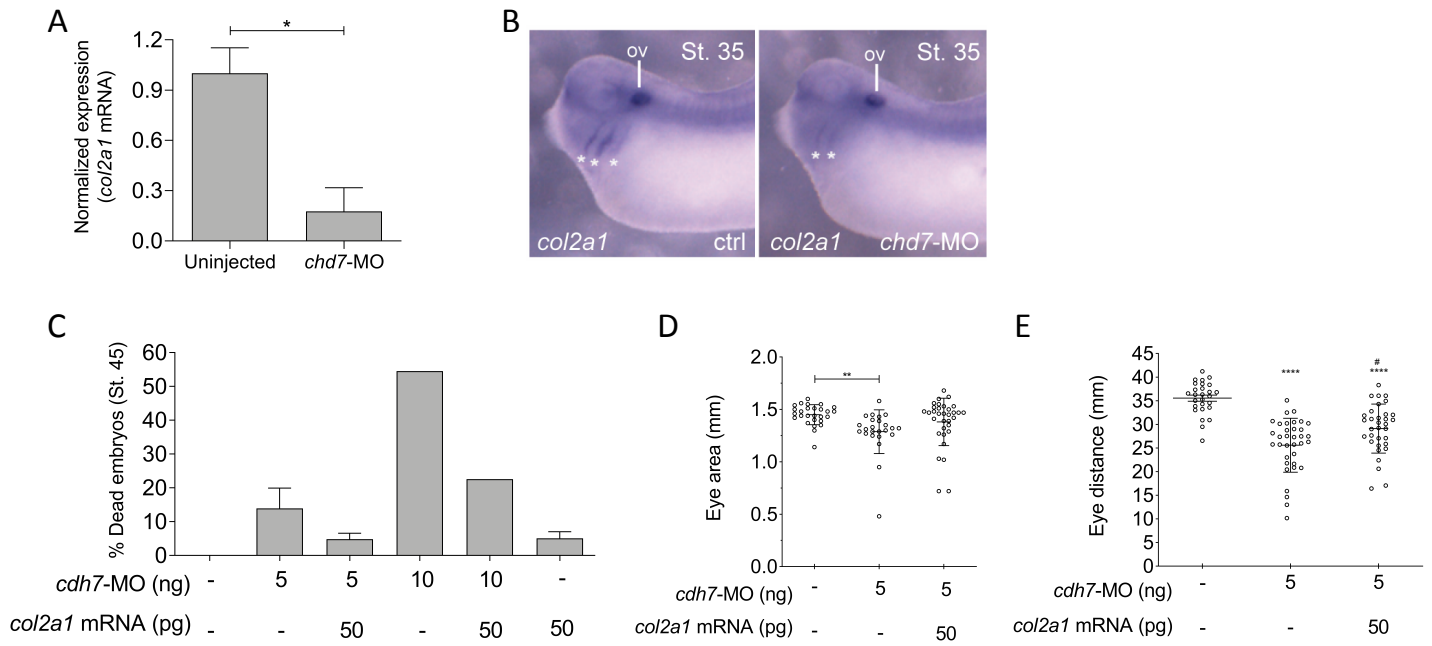

Figure 5: Expression of *col2a1* rescues Chd-7 knock-down in *Xenopus* embryos. A) Expression levels of *col2a1* mRNA are reduced in *chd7*-MO injected embryos. 2-cell staged embryos were injected into both blastomeres with 5 ng of *chd7*-MO. Error bars indicate standard error from two repeats of the PCR reaction with different biological samples. Statistical significant differences were determined by a one-tailed paired t-test (* $p < 0.05$). **B)** *Col2a1* expression is reduced in the branchyal arches of Chd7-depleted embryos. *In situ* hybridization of stage 35 embryos for *col2a1*, lateral views. 8-cell staged embryos were injected into one D1 blastomeres with 2.5 ng of *chd7*-MO. Left and right panels are control and injected sides of the same embryo, respectively. Reduced staining of the branchyal arches (asterisks) was observed in 56% of the injected embryos (N = 1, 22) (N = number of experiments, number of embryos). ov: otic vesicle. Representative embryo is shown. **C)** Lethality in Chd-7-depleted embryos is rescued by over-expression of *col2a1* in *Xenopus*. Bar graph with the percentage of dead embryos by stage 45. Higher dosage of *chd7*-MO causes an increase percentage in the number of dead embryos and co-injection of *col2a1* mRNA reduces embryonic lethality. 8-cell staged embryos were injected into both D1 blastomeres with *chd7*-MO and/or *col2a1* mRNA at the indicated doses and scored for survival at stage 45. Uninjected (N = 3, 84); *chd7*-MO 5 ng (N = 2, 64); *chd7*-MO 5 ng + *col2a1* mRNA 50 pg (N = 2, 61); *chd7*-MO 10 ng (N = 1, 33); *chd7*-MO 10 ng + *col2a1* mRNA 50 pg (N = 1, 31) and *col2a1* mRNA 50 pg (N = 2, 58). (N = number of experiments, number of embryos). **D)** Quantification of the eye area of *Xenopus* stage 45 embryos. 8-cell staged embryos were injected into both D1 blastomeres with *chd7*-MO or co-injected with *chd7*-MO and *col2a1* mRNA at the indicated doses. Means and standard deviation are indicated. Each dot represents a single embryo. Uninjected (N = 1, 27); *chd7*-MO 5 ng (N = 1, 24) and *chd7*-MO 5 ng + *col2a1* mRNA 50 pg (N = 1, 33). Statistical significant differences were determined by a one-way ANOVA and means between groups were compared using Tukey's multiple comparisons test (** $p < 0.01$). **E)** Quantification of the eye distance of *Xenopus* stage 45 embryos. 8-cell staged embryos were injected into both D1 blastomeres with *chd7*-MO or co-injected with *chd7*-MO and *col2a1* mRNA at the indicated doses. Means and standard deviation are indicated. Each dot represents a single embryo. Uninjected (N = 1, 27); *chd7*-MO 5 ng (N = 2,

35) and *chd7*-MO 5 ng + *col2a1* mRNA 50 pg (N = 1, 33). Statistical significant differences were determined by a one-way ANOVA and means between groups were compared using Tukey's multiple comparisons test (**** $P < 0.0001$, $^{\#}P < 0.05$). * represents the comparison to the uninjected group and $^{\#}$ represents the comparison to the *chd7*-MO injected group.